

Article

Renewable Hydrogen from Ethanol Reforming over CeO₂-SiO₂ Based Catalysts

Vincenzo Palma, Concetta Ruocco * , Eugenio Meloni and Antonio Ricca

Department of Industrial Engineering, University of Salerno, Via Giovanni Paolo II 132, 83040 Fisciano (SA), Italy; vpalma@unisa.it (V.P.); emeloni@unisa.it (E.M.); aricca@unisa.it (A.R.)

* Correspondence: cruocco@unisa.it; Tel.: +39-089-964-027

Received: 14 June 2017; Accepted: 26 July 2017; Published: 27 July 2017

Abstract: In this research, a bimetallic Pt-Ni/CeO₂-SiO₂ catalyst, synthetized via wet impregnation, was successfully employed for the oxidative steam reforming of ethanol between 300 and 600 °C. The reaction performance of the Pt-Ni catalyst was investigated and compared with the Ni/CeO₂-SiO₂, Pt/CeO₂-SiO₂ as well as CeO₂-SiO₂ sample. The bimetallic catalyst displayed the best results in terms of hydrogen yield and by-products selectivity, thus highlighting the crucial role of active species (Pt and Ni) in promoting ethanol conversion and reaching the products distribution predicted by thermodynamics. The most promising sample, tested at 500 °C for more than 120 h, assured total conversion and no apparent deactivation, demonstrating the stability of the selected formulation. By changing contact time, the dependence of carbon formation rate on space velocity was also investigated.

Keywords: hydrogen; ethanol oxidative steam reforming; ceria; coke

Highlights:

- CeO₂-SiO₂ displayed low hydrogen yield below 600 °C, with a relevant by-product selectivity.
- Monometallic Pt and Ni sample displayed similar results for ESR between 300 and 600 °C.
- The Pt-Ni catalyst displayed excellent stability at 500 °C, H₂O/EtOH = 4 and O₂/EtOH = 0.5.
- The Pt-Ni sample was tested to study the effect of contact time on carbon formation.

1. Introduction

A promising strategy to mitigate the environmental impacts brought by the massive use of fossil fuels consists in the choice of hydrogen as the future energy source for transportation, fuel cells and power stations [1,2]. Several technologies have been developed for hydrogen production, including electrolysis, photolysis and thermolysis of water, biological reactions, gasification and pyrolysis of biomass, steam reforming and partial oxidation of hydrocarbons [3–5]. However, the comparison among the different available processes (in terms of energy efficiency) encourages fossil fuels reforming and nowadays almost the totality of hydrogen is produced in this way [6]. Therefore, in response to the exhaustion of fossil fuels and greenhouse as well as toxic gases emission (CO₂, SO₂, NO_x), the catalytic conversion of biofuels via reforming seems to be one of the most promising alternatives towards a sustainable development. In this scenario, bio-ethanol produced from biomass, originating from agriculture (first generation bio-ethanol), forestry and urban residues (second generation bioethanol), can complement fossil fuel usage: biomass, in fact, is a relatively cheap feed-stock (some biomass by-products are almost free), helps to mitigate CO₂ emissions and is well-known for its low sulphur content [7,8]. Fermentation of lignocellulosic materials produces a water-ethanol mixture (10–18 wt % in ethanol [9]), which provides a feed that can be directly used in the steam reforming processes. From the thermodynamic standpoint, ethanol steam reforming (ESR) is favored at high temperature

and low pressure, since it is an endothermic reaction and proceeds with an increasing moles number. However, hydrogen production, depending on the operative conditions as well as catalyst choice, can be accompanied by side-products formation (including acetaldehyde, methane, ethylene, carbon monoxide [10]), as a result of the several reaction pathways occurring. Ethanol can be dehydrogenated to acetaldehyde, dehydrated to ethylene or decomposed to methane and carbon dioxide [11,12]; Boudouard reaction, C₂H₄ polymerization and CH₄ decomposition are the main causes for coke formation on the catalyst surface, a serious concern of the ESR process [13,14]. At that end, oxidative steam reforming (OSR, Equation (2)) of ethanol, which combines steam reforming and partial oxidation, is more effective in keeping clean the catalyst from carbon; moreover, compared to the conventional steam reforming reaction, a considerable improvement in energy efficiency can be achieved [15]. Among the catalysts tested so far for ethanol reforming, transition metals (Ni and Co), able to promote C-C, C-H and C-O bond cleavage [16,17], are very interesting while noble metals (Pt, Pd, Rh) are well-known for their high water gas shift activity and low susceptibility to coke formation [18]. On the other hand, several authors found that the combination of two metals (Ni-Co [19], Rh-Co [20], Cu-Ni [21,22], Pt-Ni [23,24], Pt-Co [25], Rh-Pt [18]) may improve the catalyst performance in the ethanol steam reforming reaction: the addition of a second metal plays a crucial role in enhancing reducibility, preventing sintering and limiting deactivation due to coke formation. However, few studies are focused on the choice of bimetallic formulations for oxidative steam reforming of ethanol [26–28]. Among oxide supports, alumina is commonly employed during reforming reactions owing to its mechanical and chemical stability; however, Al₂O₃ promotes ethylene production, which can easily polymerize and form coke precursors [29,30]. Conversely, rare earth based oxides, due to the high oxygen mobility and the promotion of strong metal-support interactions, may prevent sintering and deactivation by coke deposits [31]: the formation of oxygen vacancies is based on the reversible redox reaction between Ce⁴⁺ and Ce³⁺ ions, depending on the oxygen excess or defect in the environment [32]. Cifuentes et al. [33] evaluated the performances of Rh-Pt catalysts on different supports, finding that CeO₂ allowed the highest hydrogen production, followed by La₂O₃ and ZrO₂. The promotion of Ni/Al₂O₃ catalysts by CeO₂, ZrO₂ and CeO₂-ZrO₂ addition was an efficient route to increase H₂ yield and reduce coke formation: the higher number of surface oxygen species improves the carbon oxidation [34]. For Ni/SiO₂ catalysts, it was also found that Ce incorporation into the structure could reduce coke formation, due to the presence of oxygen vacancies able to promote gasification reactions [14]. The mixed oxides ceria-silica, in fact, are characterized by improved mobility of surface oxygen with respect to ceria alone [35]; the high surface area of SiO₂ materials also allows a better active species dispersion on ceria support, with a consequent enhancement of catalytic performances [36].

In our previous studies, we effectively employed Pt-Ni catalysts supported on rare earth based oxides for the ethanol steam and oxidative steam reforming reactions. However, to the best of our knowledge, the catalytic performances of monometallic Ni-based or Pt-based samples as well as of the bare support for OSR have not been investigated. Therefore, in the present work, the activity of a previously developed bimetallic catalyst (Pt-Ni/CeO₂-SiO₂, successfully employed in an ethanol membrane reformer [37,38]) was compared with the CeO₂-SiO₂, Ni/CeO₂-SiO₂ and Pt/CeO₂-SiO₂ samples, in order to highlight the role of the active species in the oxidative reforming reaction. The bimetallic catalyst was also employed for stability tests at 500 °C, S/E = 4 and O₂/E = 0.5 at different contact times and for considerable time-on-stream (TOS), with the aim of evaluating the impact of space velocity on carbon selectivity.

2. Catalyst Preparation and Characterization

CeO₂-SiO₂ was used as support material and prepared by wet impregnation from an aqueous solution 1.5 M of Ce(NO₃)₃·6H₂O (Strem Chemicals, Newburyport, MA, USA). The impregnation of SiO₂ (90–115 µm, Sigma-Aldrich, Saint Louis, MO, USA), previously calcined in air at 600 °C for 3 h (heating rate of 10 °C·min⁻¹), was carried out at 80 °C for 2 h. The recovered solid was dried overnight at 120 °C and calcined at 600 °C for 3 h (heating rate of 10 °C·min⁻¹). Nickel was loaded

on the CeO₂-SiO₂ support by the above method; Ni(NO₃)₂·6H₂O (Strem Chemicals) was used as salt precursor. The proper amount of nickel nitrate hexahydrate was dissolved in water, and then the impregnation of CeO₂-SiO₂ sample was performed on a stirred and heating plate as described for ceria deposition on silica. Pt was deposited on the Ni/CeO₂-SiO₂ catalyst (or on the bare CeO₂-SiO₂ support) by the same procedure and the final loadings were 30 wt % CeO₂ and 10 wt % Ni as well as 3 wt % Pt calculated with respect to ceria mass.

The chemical composition of each sample was determined by the X-ray fluorescence (XRF) method on an ARL (Air Resources Laboratory) QUANTX ED-XRF (energy-dispersive X-ray diffraction) spectrometer (Thermo Fisher Scientific, Waltham, MA, USA). The measurement technique applied was based on a calibration curve obtained using standards.

The Brunauer-Emmett-Teller (BET) surface area of each sample was determined by N₂ adsorption at −196 °C (Sorptometer 1040 “Kelvin” from Costech Analytical Technologies, Valencia, CA, USA) after outgassing the sample at 150 °C for 2 h.

The crystalline phases of the support and the final catalysts were measured by X-ray diffraction (XRD) analysis using a Rigaku diffractometer (The Woodlands, TX, USA) having Cu K radiation ($\lambda = 1.5406 \text{ \AA}$) over a 2θ range of 20–80°.

Reducibility of the prepared samples was studied by Temperature Programmed Reduction (TPR) with hydrogen. The catalyst was loaded in the tubular reactor described in Section 3 and gases were supplied to the reactor chamber with calibrated mass flow-controllers. Nitrogen (500 Ncm³·min^{−1}) was flowing for 20 min before the flow was switched to 5% H₂/N₂ (500 Ncm³·min^{−1} up to 600 °C, heating rate of 10 °C·min^{−1}, dwell time at 600 °C of 1 h).

The amount of carbon deposited on the spent catalysts was determined using a thermogravimetric analyzer (TA Instrument Q600 coupled with PFEIFFER ThermoStar Quadrupole Mass Spectrometer, New Castle, DE, USA). Approximately 20 mg of the used catalyst was heated from room temperature to 1000 °C with a heating rate of 10 °C·min^{−1} in air.

3. Catalytic Performance Evaluation

Ethanol OSR was performed in a continuous fixed bed stainless steel reactor at atmospheric pressure, H₂O/EtOH = 4 mol/mol (10 vol % of ethanol), O₂/EtOH = 0.5 mol/mol, WHSV (weight hourly space velocity calculated as the ratio between ethanol mass flow-rate and catalytic mass) of 4.1–123 h^{−1} and a range of temperature between 300 and 600 °C. Before setting up the reaction, the catalysts were reduced “in situ” as described in Section 2. In a typical catalytic test, the reactor is loaded with 4.5 g (3 cm³) of powder catalysts (crushed and sieved to reach a particle size in the range of 180–355 μm). Temperature can be measured through a K-thermocouple in correspondence of the catalyst end section while a differential pressure sensor monitors the pressure drops across the catalytic bed. The water and ethanol can be fed together from a tank pressurized at 6 bar with a mass flow meter/controller Bronkhorst Liqui-Flow. After the heating under a N₂ stream of 500 Ncm³·min^{−1}, the screening tests on the monometallic and bimetallic catalysts were performed by decreasing the temperature from 600 to 300 °C with a rate of 10 °C·min^{−1}. The same procedure was followed for stability tests and performed at fixed temperature (500 °C). The gas products were analyzed using a Fourier Transform Infrared (FT-IR) Spectrophotometer (IGS Antaris by Thermo Scientific, Waltham, MA, USA). The reactor’s off-gas was cooled via two condenser units and sent to an ABB block (Analytical Measurement ABB Group, Alamo, TX, USA), equipped with a CALDOS-27 having a thermal conductivity detector to record online H₂ concentration while the paramagnetic detector of the MAGNOS-206 allowed monitoring O₂ signal. Overall carbon and hydrogen balances in most cases closed within ±10%; larger errors were only observed over the bare support and at T < 350 °C.

A series of experiments were carried out at different temperatures and contact time. The performances of the catalyst were evaluated by determining the conversion of ethanol X (Equation (1)), yield of hydrogen Y (Equation (2)), main carbon-containing products (CO, CO₂ and CH₄) selectivity S_i (Equation (3)) and carbon formation rates CFR (Equation (4)), where *mass_{coke}* (m_c in grams)

is determined through thermo-gravimetric analysis, $mass_{catalyst}$ (m_{cat} in grams) stands for the catalytic mass, $mass_{carbon,fed}$ ($m_{c,fed}$ in grams) refers to the total mass of carbon fed as ethanol during the test and TOS is the time-on-stream (in hours), as defined below:

$$X = \frac{moles_{C_2H_5OH,in} - moles_{C_2H_5OH,out}}{moles_{C_2H_5OH,in}} \times 100 \quad (1)$$

$$Y = \frac{moles_{H_2}}{6 \cdot moles_{C_2H_5OH,in}} \times 100 \quad (2)$$

$$Si = \frac{moles_i}{2 \cdot (moles_{C_2H_5OH,in} - moles_{C_2H_5OH,out})} \times 100 \quad (3)$$

$$CFR = \frac{mass_{coke}}{mass_{catalyst} \cdot mass_{carbon,fed} \cdot TOS} \quad (4)$$

4. Catalysts Characterization

The physiochemical properties of the calcined support, the monometallic samples as well as Pt-Ni/CeO₂-SiO₂ are shown in Table 1. The content of the different elements and oxides incorporated to the samples, determined by XRF analysis, are very close to the nominal values, taking into account that, for example in the case of the bimetallic catalyst, 3.5 and 1 wt % of the metals in the mixed oxide means a nominal loading of Ni and Pt with respect to ceria of 10 and 3 wt %, respectively. All the samples displayed very high specific surface areas: SiO₂ inclusion (BET surface area after calcination at 600 °C for 3 h of 400 m²·h⁻¹) in the matrices with CeO₂ carrier promotes an improvement in surface area, which is expected to enhance active species dispersion and catalytic performances [36]. Moreover, it is interesting to note that active species deposition was not responsible for pore blocking: in fact, the three samples displayed almost the same surface area. The X-ray diffraction patterns of the calcined catalysts are reported in Figure 1. All samples show a broad peak in the 2θ region of 20–30°, attributed to the amorphous silica [39]. In addition, they clearly display the diffraction peaks corresponding to CeO₂, that well match with the peaks of the fluorite cubic phase [40]. Calcined Ni samples exhibit diffraction peaks at 2θ = 37.3° and 43.3° corresponding to the planes (1 1 1) and (2 0 0) of the face-centered cubic structure of NiO, respectively [41,42]. In the insertion of Figure 1, the magnification of the NiO peaks at 43.3°, used for the calculation of average crystallite sizes, was reported. The lack of diffraction peaks related to Pt phases could be attributed to low loading of metal, small size of Pt crystallites and high dispersion of metal particles [43]. The results of TEM-EDAX Transmission Electron Microscope-Energy Dispersive Analysis X-ray Spectroscopy (FEI Tecnai F20, San Martino Buon Albergo, Italy) analysis (discussed in a previous work and not shown), displayed that Pt signal is linked to Ni particles and this result suggests the formation of a solid solution between Pt and Ni [44]. However, no shift peak was observed in the XRD spectra (Figure 1) and only signals ascribable to NiO are visible. In fact, the amounts of Pt-Ni solid solution eventually present is beneath the detection limit of XRD.

The average sizes of ceria crystallites (Table 1), evaluated by means of the Scherrer formula, is almost the same in the four samples, proving that active species deposition (and the further calcination step) had no effect on CeO₂ dispersion. On the other hand, the deposition of platinum on Ni/CeO₂-SiO₂ catalyst resulted in a better dispersion of NiO crystallites: the lower sizes of nickel oxide particles in noble metals promoted catalysts, previously observed [45], and can be linked to formation of a Pt-Ni solid solution, which improved NiO dispersion.

TPR measurements were aimed at characterizing the reducibility of oxide phases present in the mono- and bimetallic catalysts. The results were compared with the hydrogen consumption profile of bare support (CeO₂-SiO₂) and the quantitative results of TPR analysis are shown in Table 2. The broad peaks observed in Figure 2 were deconvoluted in symmetrical peaks to evaluate the relative percentage of the different reducible species. The deconvolution was carried out by means of the Origin software

(using Gaussian multipeaks curve-fitting) and the deconvoluted profiles were reported in Figure 2. The results of the experiments (Figure 2) demonstrate that the catalysts easily undergo reduction with hydrogen. The $\text{CeO}_2\text{-SiO}_2$ sample displayed hydrogen consumption between 250 and 550 °C, assigned to the surface reduction $\text{Ce}^{4+} \rightarrow \text{Ce}^{3+}$ of cerium ions [46,47] and the total H_2 uptake correspond to 298 $\mu\text{mol/g}_{\text{cat}}$ (Table 2).

Table 1. Chemical composition and structural properties of the as-prepared samples.

Sample	SSA ($\text{m}^2\cdot\text{g}^{-1}$)	wt % CeO_2	wt % Ni	wt % Pt	d_{CeO_2} (nm)	d_{NiO} (nm)
Si	400	-	-	-	-	-
CeSi	254	31.1	-	-	78	-
NiCeSi	256	30.8	3.5	-	74	112
PtCeSi	253	30.8	-	1.1	76	-
PtNiCeSi	255	30.3	3.4	1	73	85

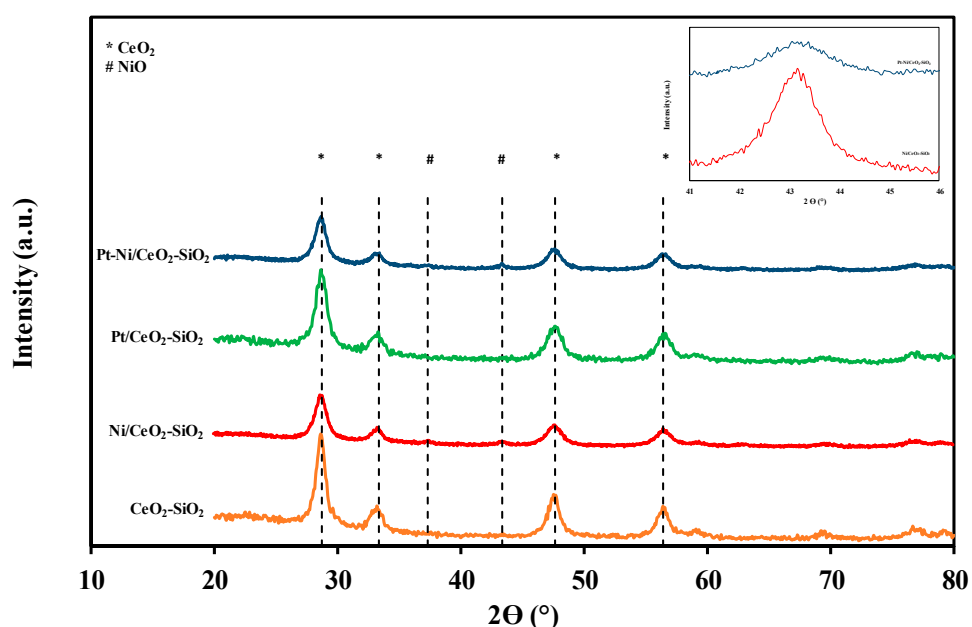


Figure 1. X-ray diffraction (XRD) spectra of calcined support, mono- and bi-metallic catalysts.

The monometallic catalyst without Pt showed a much more complex reduction profile with various peaks in the range 200–500 °C. As previously reported, the low-temperature zone (which comprises the peaks located at 237 and 289 °C) is ascribed to the adsorbed oxygen reduction [48]. However, the contribution of bulk NiO particles reduction dispersed on ceria support cannot be excluded [49]. The peak observed in the middle-temperature zone at 334 °C can be correlated to the reduction of NiO interacting with (but not chemically bound to) the support; finally, the peak observed at 435 °C can be associated to the formation of Ni-Ce solid solution and/or to the reduction of CeO_2 surface oxygen, shifted towards lower temperature due to H_2 spillover promoted by Ni [26,50]. The total H_2 consumption measured over the monometallic Ni-catalyst was lower (1424 vs. 1704 $\mu\text{mol/g}_{\text{cat}}$) than that required for the total reduction of NiO. This result suggests that nickel oxide particles have a different interaction degree with the support and strong NiO- CeO_2 bonds hinder Ni reduction [51]. On the other hand, it is also possible that the easily reducible NiO particles cause spillover of hydrogen onto the support inducing a concurrent reduction of both nickel oxide and the surface of ceria [52,53]. For the monometallic Pt-based sample, the main hydrogen consumption (424 $\mu\text{mol/g}_{\text{cat}}$) was observed below 220 °C; two broad peaks were also observed at 308 and 403 °C, accounting, however, for a very low hydrogen uptake. These results demonstrate that PtO_x phases are mainly

present in a well-dispersed form. The catalyst containing both Pt and Ni exhibited a rearrangement of the reduction profile: the hydrogen consumption was shifted towards lower temperatures compared to the monometallic catalysts. The peak observed at 109 °C is associated with the reduction of the surface PtO_x phase. However, the main H_2 consumption peak observed at $T < 200$ °C may result from the reduction of a PtNi [44] alloy or by means of the just reduced Pt particles, able to provide dissociate hydrogen (H_2 spillover) for reducing nearby NiO phases [54]. In fact, the total hydrogen uptake in the low temperature range (1062 $\mu\text{mol/g}_{\text{cat}}$) is much higher than that required for the complete reduction of PtO_x species (308 $\mu\text{mol/g}_{\text{cat}}$). As previously observed, the interaction of Ni with a noble metal results in an easier reduction of the non-noble metal, shifting, at the same time, the characteristic reduction peaks towards lower temperatures than that observed for the $\text{Ni/CeO}_2\text{-SiO}_2$ sample [55]. Hydrogen spillover resulted in a total hydrogen uptake of 2735 $\mu\text{mol/g}_{\text{cat}}$ (Table 2, against a theoretical value of 2012 $\mu\text{mol/g}_{\text{cat}}$): the enhancement of CeO_2 reduction, observed at lower temperatures than that recorded over the bare support, is promoted by the metals-support interaction, which weakened the Ce-O bond, thus increasing the mobility of lattice oxygen [56–58].

Table 2. Quantitative results of TPR analysis.

Sample	T (°C)	H_2 Uptake ($\mu\text{mol/g}_{\text{cat}}$)
$\text{CeO}_2\text{-SiO}_2$	300	13
	448	94
	509	191
$\text{Ni/CeO}_2\text{-SiO}_2$	237	36
	289	103
	388	551
	435	734
$\text{Pt/CeO}_2\text{-SiO}_2$	149	137
	190	287
	308	35
	403	50
$\text{Pt-Ni/CeO}_2\text{-SiO}_2$	109	119
	179	943
	334	1032
	366	641

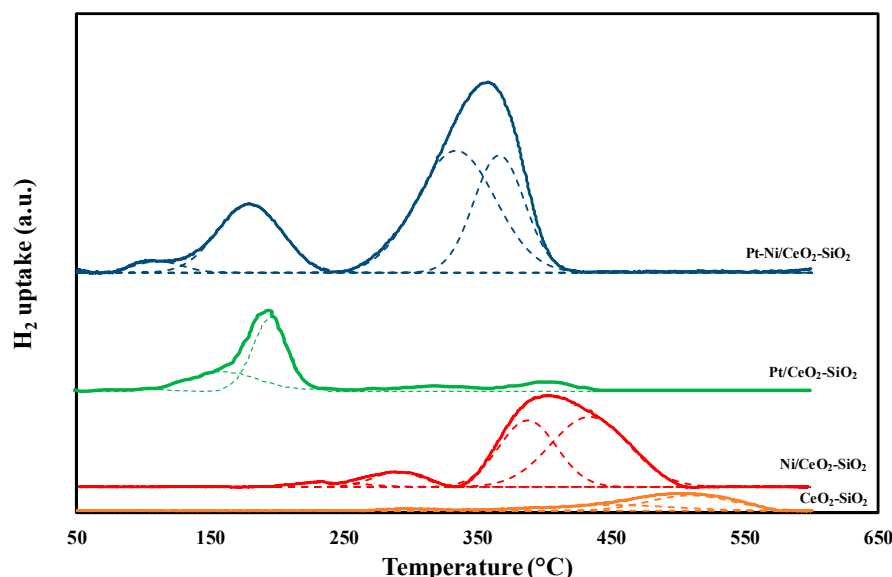


Figure 2. Temperature Programmed Reduction (TPR) profile of calcined support, mono- and bi-metallic catalysts after baseline subtraction (the deconvoluted peaks were represented by dotted lines).

5. Catalytic Performances of CeO₂-SiO₂ Based Samples

The experimental results of ethanol OSR tests were compared with thermodynamic predictions evaluated by means of the software GasEQ (<http://www.c.morley.dsl.pipex.com>), based on the minimization of free Gibbs energy for the calculation of chemical equilibrium. Thermodynamics predicts total conversion (not shown) in the whole temperature interval while the equilibrium S_i and Y values are depicted in Figure 3. The activity performances of the investigated catalysts are illustrated in terms of ethanol conversion and hydrogen yield as a function of reaction temperature in Figure 4a,b, respectively; the catalytic activity of CeO₂ was taken as reference. For mono- and bimetallic samples, ethanol conversion increased with temperature, easily reaching the total EtOH conversion within 450 °C; conversely the bare support did not overcome a fuel conversion of 96% also for an operating temperature of 600 °C.

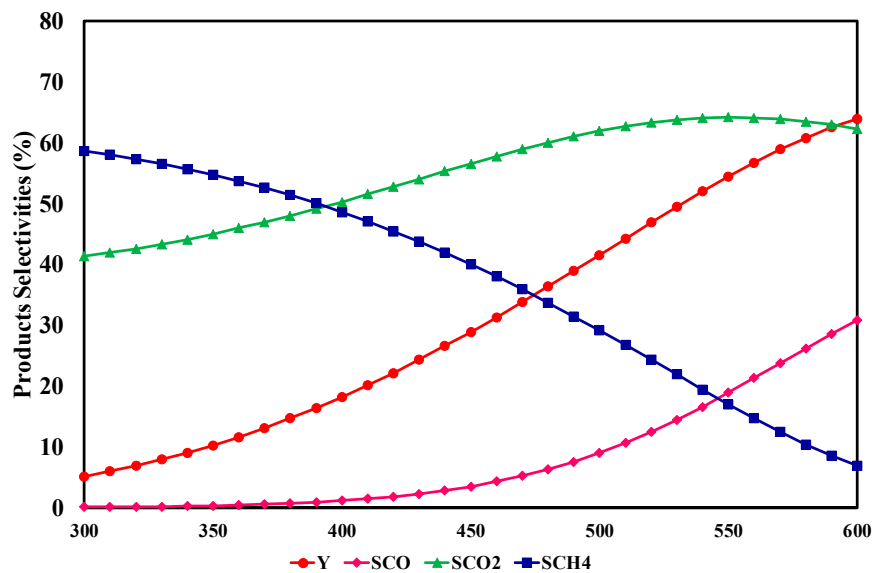


Figure 3. Hydrogen yield and CO, CO₂ and CH₄ selectivities as a function of reaction temperature predicted by thermodynamic equilibrium; H₂O/EtOH = 4, O₂/EtOH = 0.5.

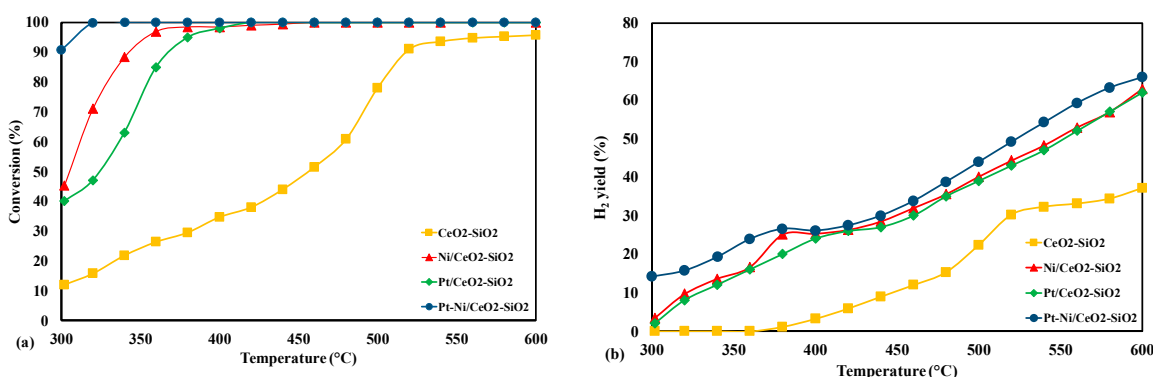


Figure 4. Ethanol conversion (a) and hydrogen yield (b) vs. temperature over the calcined support, mono- and bi-metallic catalysts; H₂O/EtOH = 4, O₂/EtOH = 0.5, WHSV = 4.1 h⁻¹.

The monometallic Ni-based catalysts displayed a total conversion above 450 °C and a non-negligible ethanol concentration in the reforming mixture between 360 and 450 °C. Above 400 °C, the performances of the two monometallic catalysts were comparable. However, by lowering the reaction temperature, decreased activity was recorded over the Pt/CeO₂-SiO₂ catalyst, which reached

$X = 40\%$ at $300\text{ }^{\circ}\text{C}$. On the other hand, a conversion of 45% and 93% was recorded at $300\text{ }^{\circ}\text{C}$ over the Ni and Pt-Ni based catalysts, respectively. In fact, Pt addition to $\text{Ni}/\text{CeO}_2\text{-SiO}_2$ catalyst strongly improved activity in the whole temperature interval, assuring total ethanol conversion at $T > 320\text{ }^{\circ}\text{C}$. In terms of hydrogen yield, as predicted by thermodynamic equilibrium, an increased hydrogen production was observed at high temperatures over the three catalysts. H_2 yield ranged between 31 and 35.3% above $520\text{ }^{\circ}\text{C}$ over the $\text{CeO}_2\text{-SiO}_2$ support.

However, enhanced H_2 yields were recorded after active species deposition: very close profiles were observed between 400 and $440\text{ }^{\circ}\text{C}$ over the mono- and bimetallic catalysts; once again, the best results in terms of H_2 production were assured by the $\text{Pt-Ni}/\text{CeO}_2\text{-SiO}_2$ sample.

In order to investigate in depth the effect of active species on catalytic performances of $\text{CeO}_2\text{-SiO}_2$ -based catalysts, the results were also compared in terms of main carbon-containing species selectivity (Table 3). At $600\text{ }^{\circ}\text{C}$, a non-negligible hydrogen production was observed over the bare support ($Y = 35.3\%$), which, however, displayed a quite high CH_4 selectivity, demonstrating the key role of active components in promoting reforming reactions. By lowering the temperature, the reduction in methane selectivity from 26.9 to 12.8% was matched by a growth in the H_2 as well as CO_2 selectivity (which may indicate the promotion of CH_4 steam reforming reaction): these results suggest that lower temperatures are in favor of by-product formation. Coke precursors (CH_x) can be easily formed [59] through methane decomposition reaction, and, in addition, acetaldehyde was also detected among the reaction products even at $600\text{ }^{\circ}\text{C}$. Ni deposition on $\text{CeO}_2\text{-SiO}_2$ support strongly increased H_2 production in the whole temperature interval, due to the enhanced contribution of both methane steam reforming and water gas shift reaction (at 500 and $400\text{ }^{\circ}\text{C}$): as a result, CH_4 selectivity decreased from 26.9 to 9.9% at $600\text{ }^{\circ}\text{C}$ and S_{CO} reached 10.5% at $500\text{ }^{\circ}\text{C}$.

Table 3. Hydrogen yield and main carbon-containing products selectivity during reforming tests at $\text{H}_2\text{O/EtOH} = 4$, $\text{O}_2/\text{EtOH} = 0.5$, WHSV = 4.1 h^{-1} .

Sample	T ($^{\circ}\text{C}$)	Y (%)	S_{CH_4} (%)	S_{CO} (%)	S_{CO_2} (%)
$\text{CeO}_2\text{-SiO}_2$	600	35.3	26.9	20.1	50.4
	500	22.2	12.8	44.5	26.1
	400	3.5	0	21.2	29.4
	300	0	0	4.6	46.9
$\text{Ni}/\text{CeO}_2\text{-SiO}_2$	600	60.2	9.9	31.2	58.9
	500	40.1	35.9	10.5	53.6
	400	26.1	44.1	1.9	53.2
	300	3.1	28.7	10.4	6.2
$\text{Pt}/\text{CeO}_2\text{-SiO}_2$	600	62.2	8.9	33.2	57.9
	500	39.1	35.1	12.6	52.3
	400	24.3	42.1	3.2	51.9
	300	2.1	29.2	5.6	5.8
$\text{Pt-Ni}/\text{CeO}_2\text{-SiO}_2$	600	65.2	6.7	30.8	62.5
	500	42.1	29.1	8.8	62.1
	400	26.5	44.2	1.7	54.1
	300	13.1	38.7	6.4	37.3

However, the unclosed carbon balances at 300 and $400\text{ }^{\circ}\text{C}$, as well as acetaldehyde traces detected in the reaction products, suggest that by-products (including coke) selectivity increases at low temperatures also on the $\text{Ni}/\text{CeO}_2\text{-SiO}_2$ catalyst. On the other hand, product gas distribution observed over the two monometallic catalysts was similar above $400\text{ }^{\circ}\text{C}$ while, by reducing the reaction temperature, slightly bad performances were recorded over the $\text{Pt}/\text{CeO}_2\text{-SiO}_2$ catalyst: this result suggests a quite high by-product selectivity (acetone traces were recorded in the mixture exiting the reactor) over the Pt-based catalyst at $T < 400\text{ }^{\circ}\text{C}$. In fact, only Pt addition drove the system towards the thermodynamic equilibrium, which was followed with a fairly good agreement until $420\text{ }^{\circ}\text{C}$.

In particular, the quite high CO selectivity observed at 600 °C, demonstrates that the role of water gas shift reaction is negligible at high temperatures, as predicted by thermodynamics, due to the reaction exothermicity. Moreover, for total ethanol conversion, it is noticeable from Table 3 that Ni-based catalysts assures a lower CO selectivity, thus suggesting a higher rate of WGS reactions. As a result, improved H₂ yields were observed. In the middle temperature interval, the hydrogen yield exceeded thermodynamic predictions on both Ni/CeO₂-SiO₂ and Pt-Ni/CeO₂-SiO₂ catalysts: as previously observed [36], the reaction mechanism is very complex and, below 420 °C, the system kinetically is not able to reach equilibrium values.

Combining the results shown in Figure 4a,b as well as Table 3, it becomes clear that the synergy between Ni and Pt can lead to a great increase in catalyst activity, pointing out the formation of a platinum solid solution in the structure of Ni, discussed above. The synergy between the two metals, also attested by enhanced catalyst reducibility during TPR results, was shown to maintain the catalyst activity for a long period of time [60–62]. In fact, Pt deposition on Ni/CeO₂-SiO₂ catalyst strongly reduces carbon formation tendency [63]. In addition, as shown in Table 1, Pt addition favors the formation of smaller nickel oxide particles, increasing catalyst performance for reforming reaction.

The product gas distribution as a function of TOS was investigated over the most promising sample at 500 °C, water/ethanol and oxygen/ethanol molar ratio of 4 and 0.5, respectively; space velocity was preliminary fixed to 4.1 h⁻¹. During oxidative steam reforming, the main products were CH₄, CO, CO₂ and H₂: a stable behavior was observed for more than 120 h and products selectivity well agreed with thermodynamic predictions (Figure 5). Only ethanol traces were detected in the product mixture after 135 h of TOS, demonstrating that, at the selected operative conditions, the available amount of catalyst is able to completely convert ethanol for several hours without apparent deactivation. However, the concentration trend observed at 150 h suggests a decreased contribution of steam reforming reaction, ascribable to a catalyst loss of activity. Despite the negligible pressure drops variation through the bed (indicative of carbonaceous deposit formation which can cause reactor plugging), coke accumulation on the catalyst surface was attested by thermogravimetric analysis (TGA) results, which revealed a carbon formation rate of 1.2×10^{-6} g_{coke}·g_{c,fed}⁻¹·g_{cat}⁻¹·h⁻¹. At similar operative conditions (which means a similar ratio between feed and catalytic mass), other authors found a faster deposition of coke [28,64], even if stability tests were performed for lower TOS [65]: these results demonstrated the competitiveness of the Pt-Ni/CeO₂-SiO₂ catalyst in terms of endurance performances. In order to evaluate catalyst stability under more stressful conditions, space velocity was increased from 4.1 to 123 h⁻¹ and the effect of contact time on ethanol conversion was investigated. The catalyst was held at a fixed space velocity for 20 min; after that, total flow-rate was adjusted to reach the subsequent desired WHSV. At 61.5 h⁻¹ (15 times the value selected for the test in Figure 5), total ethanol conversion was still recorded.

Decreased performances were observed for lower contact times, with a 99% of conversion after 20 min at 82 h⁻¹ and 89% after 20 min at 123 h⁻¹ (Figure 5). When the stability test was carried out at 123 h⁻¹ for almost 60 h starting from a fresh sample (Figure 7), initial conversion was about 98% (vs. 94% observed in Figure 6), due to the partial catalyst deactivation observed by increasing space velocity. The bimetallic catalyst, tested at a space velocity 30 times higher than that selected in Figure 5, displayed a decreasing trend of ethanol conversion (Figure 7a) from 98 to 42% during the first 40 h of TOS. Accordingly, pressure drops through the bed increased from 120 to 160 mbar (Figure 7b), attesting coke deposition during the test. After 40 h, a plateau condition was reached and no more variation in both conversion and pressure drop profile was observed. Differently from the data reported by other authors, which observed almost steady performances followed by a severe drop in ethanol conversion and finally a slow decrease in ethanol conversion until total deactivation of the Ni-based catalysts, in this work steady performances were observed [66,67]. The experimental results showed, as commonly reported in the literature, that coke accumulation in the catalytic bed causes an appreciable increase in pressure drops; it is interesting to remark that, after 40 h of TOS, the absence of growth in pressure drops evidences no carbonaceous species accumulation. As a consequence, the net

rate of carbon formation (i.e., the difference between carbon formation and gasification contributions) becomes equal to zero. These results suggest that the carbonaceous deposits accumulated during the test may cause, in turn, the deactivation of the active sites, which are involved in coke precursor formation themselves.

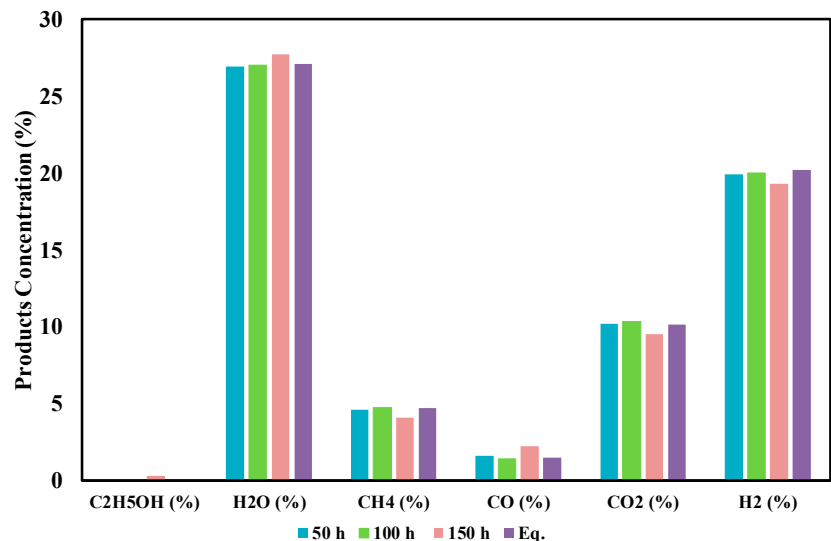


Figure 5. Results of stability test performed over Pt-Ni/CeO₂/SiO₂ catalyst at 500 °C, H₂O/EtOH = 4, O₂/EtOH = 0.5 and weight hourly space velocity (WHSV) = 4.1 h⁻¹.

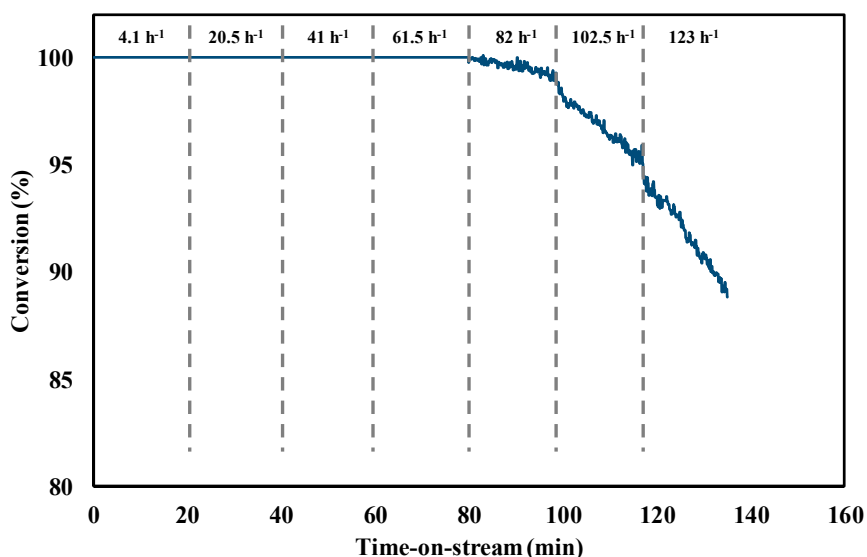


Figure 6. Results of stability test performed over Pt-Ni/CeO₂/SiO₂ catalyst at 500 °C, H₂O/EtOH = 4, O₂/EtOH = 0.5 and WHSV in the interval 4.1–123 h⁻¹.

The spent catalyst after stability test shown in Figure 8 was characterized by means of TGA, measuring a carbon formation rate of 6×10^{-5} g_{coke}·g_{c,fed}⁻¹·g_{cat}⁻¹·h⁻¹, which is almost 50 times higher than that obtained after the test at 4.1 h⁻¹. Based on these results, it is possible to conclude that carbon formation rate dependency on space velocity, as described in Figure 8, is not linear. In a previous work [68], the bimetallic Pt-Ni/CeO₂ catalyst tested under steam reforming conditions at r.a. = 6 and 450 °C, displayed a similar relationship between CFR and WHSV, proving the less relevant effect of temperature and feeding conditions while highlighting the strong impact of contact time on CFR.

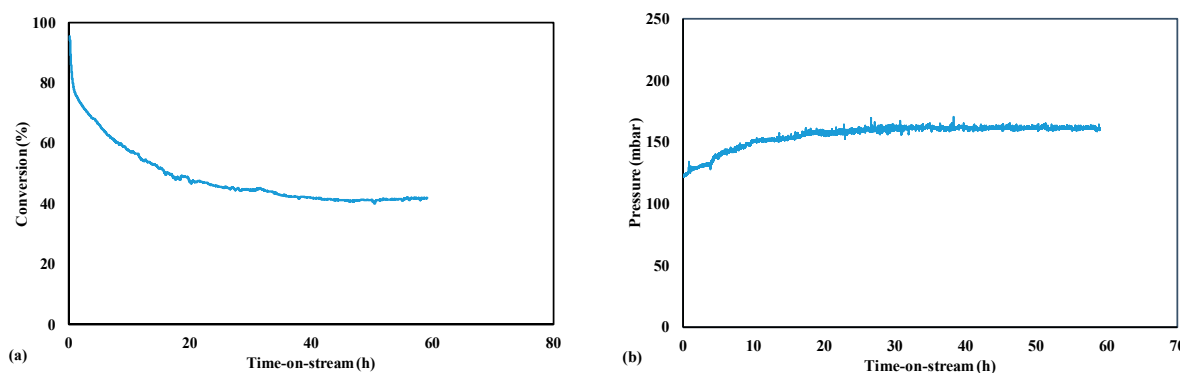


Figure 7. Ethanol conversion (a) and pressure drops profile (b) over Pt-Ni/CeO₂/SiO₂ catalyst at 500 °C, H₂O/EtOH = 4, O₂/EtOH = 0.5 and WHSV = 123 h⁻¹.

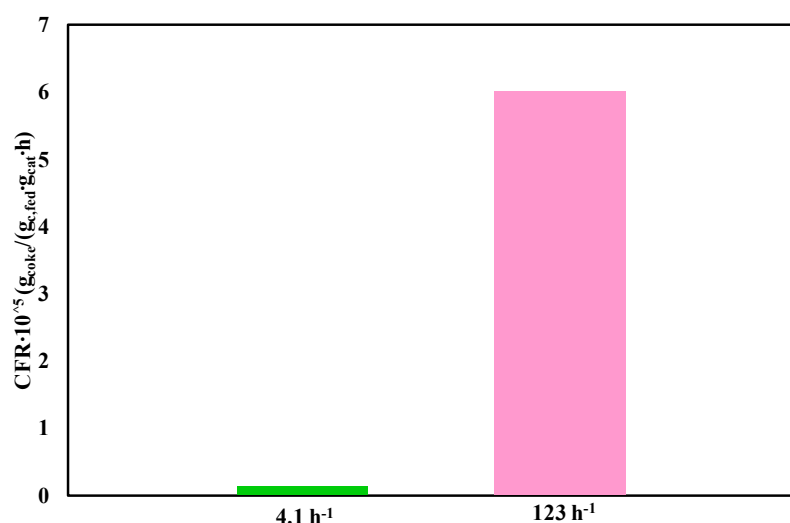


Figure 8. Dependence of carbon formation rate on WHSV; H₂O/EtOH = 4, O₂/EtOH = 0.5; T = 500 °C.

Moreover, it is worthwhile noting that several authors [15,65,69], reporting OSR tests for WHSV in the range 40–70 h⁻¹, measured CFR as higher or comparable (1.3×10^{-4} and $6.9 \times 10^{-5} \text{ g}_{\text{coke}} \cdot \text{g}_{\text{cat}}^{-1} \cdot \text{h}^{-1}$) to the value recorded over the Pt-Ni/CeO₂-SiO₂ catalyst at 123 h⁻¹. The influence of space velocity on CFR can be explained considering that the low contact time is responsible for a reduced extent of coke gasification reaction, per se already slower than the reactions in gaseous phase due to its heterogeneous nature [70].

The above result demonstrates the promising stability behavior of the bimetallic formulation.

6. Conclusions

In summary, CeO₂-SiO₂ based catalysts, prepared by the wet impregnation method and with very interesting structural properties (i.e., relatively high surface areas and good active species dispersion), has been utilized for oxidative steam reforming of ethanol (H₂O/EtOH = 4, O₂/EtOH = 0.5). Compared with the Ni/CeO₂-SiO₂ as well as the Pt/CeO₂-SiO₂ sample, the bimetallic catalyst displayed higher catalytic activity between 300 and 600 °C. Conversely, the bare support showed very low hydrogen yield, due to the relevant by-products selectivity. The Pt-Ni/CeO₂-SiO₂, tested at 500 °C and 4.1 h⁻¹, assured a stable behavior for more than 120 h, with total conversion at a fairly good agreement between experimental and equilibrium product distribution. For stability tests performed at 500 °C and 123 h⁻¹, after almost 40 h of TOS, the system reached a plateau condition where no more variation in conversion and pressure drops through the bed was observed: these results indicate that

the net rate of carbon formation was equal to zero. The relationship between CFR and WHSV was also investigated, finding a non-linear dependence.

Acknowledgments: The research leading to these results has received funding from the European Union's Seventh Framework Programme (FP7/2007-2013) for the Fuel Cells and Hydrogen Joint Technology Initiative under grant agreement no. 621196. The present publication reflects only the author's views and the FCH JU and the Union are not liable for any use that may be made of the information contained therein.

Author Contributions: Vincenzo Palma and Concetta Ruocco conceived and designed the experiments; Concetta Ruocco performed the experiments; Vincenzo Palma, Concetta Ruocco and Antonio Ricca analyzed the data; Eugenio Meloni contributed reagents/materials/analysis tools; Concetta Ruocco wrote the paper.

Conflicts of Interest: The authors declare no conflict of interest.

References

1. Wang, L.; Huang, L.; Jiao, C.; Huang, Z.; Liang, F.; Liu, S.; Wang, Y.; Zhang, H. Preparation of Rh/Ni bimetallic nanoparticles and their catalytic activities for hydrogen generation from hydrolysis of KBH₄. *Catalysts* **2017**, *7*, 125. [[CrossRef](#)]
2. Li, G.; Kanezashi, M.; Tsuru, T. Catalytic ammonia decomposition over high-performance Ru/Graphene nanocomposites for efficient CO_x-free hydrogen production. *Catalysts* **2017**, *7*, 23. [[CrossRef](#)]
3. Bär, J.; Antinori, C.; Maier, L.; Deutschmann, O. Spatial concentration profiles for the catalytic partial oxidation of jet fuel surrogates in a Rh/Al₂O₃ coated monolith. *Catalysts* **2016**, *6*, 207. [[CrossRef](#)]
4. Haryanto, A.; Fernando, S.; Murali, N.; Adhikari, S. Current status of hydrogen production techniques by steam reforming of ethanol: A review. *Energy Fuels* **2005**, *19*, 2098–2106. [[CrossRef](#)]
5. Ni, M.; Leung, D.Y.C.; Leung, M.K.H.; Sumathy, K. An overview of hydrogen production from biomass. *Fuel Process. Technol.* **2006**, *87*, 461–472. [[CrossRef](#)]
6. Jo, S.W.; Im, Y.; Do, J.Y.; Park, N.-K.; Lee, T.J.; Lee, S.T.; Cha, M.S.; Jeon, M.K.; Kang, M. Synergies between Ni, Co, and Mn ions in trimetallic Ni_{1-x}Co_xMnO₄ catalysts for effective hydrogen production from propane steam reforming. *Renew. Energy* **2017**, *113*, 248–256. [[CrossRef](#)]
7. Wang, Y.; Zou, S.; Cai, W.-B. Recent Advances on Electro-oxidation of ethanol on Pt- and Pd-based catalysts: From reaction mechanisms to catalytic materials. *Catalysts* **2015**, *5*, 1507–1534. [[CrossRef](#)]
8. Nahar, G.; Mote, D.; Dupont, V. Hydrogen production from reforming of biogas: Review of technological advances and an Indian perspective. *Renew. Sustain. Energy Rev.* **2017**, *76*, 1032–1052. [[CrossRef](#)]
9. Gaudillere, C.; González, J.J.; Chica, A.; Serra, J.M. YSZ monoliths promoted with Co as catalysts for the production of H₂ by steam reforming of ethanol. *Appl. Catal. A Gen.* **2017**, *538*, 165–173. [[CrossRef](#)]
10. Han, S.J.; Song, J.H.; Bang, Y.; Yoo, J.; Park, S.; Kang, K.H.; Song, I.K. Hydrogen production by steam reforming of ethanol over mesoporous Cu-Ni-Al₂O₃-ZrO₂ xerogel catalysts. *Int. J. Hydrogen Energy* **2016**, *41*, 2554–2563. [[CrossRef](#)]
11. González-Gil, R.; Herrera, C.; Larrubia, M.A.; Mariño, F.; Laborde, M.; Alemany, L.J. Hydrogen production by ethanol steam reforming over multimetallic RhCeNi/Al₂O₃ structured catalyst. Pilot-scale study. *Int. J. Hydrogen Energy* **2016**, *41*, 16786–16796. [[CrossRef](#)]
12. Cifuentes, B.; Figueredo, M.; Cobo, M. Response surface methodology and aspen plus integration for the simulation of the catalytic steam reforming of ethanol. *Catalysts* **2017**, *7*, 15. [[CrossRef](#)]
13. Marinho, A.L.A.; Rabelo-Neto, R.C.; Noronha, F.B.; Mattos, L.V. Steam reforming of ethanol over Ni-based catalysts obtained from LaNiO₃ and LaNiO₃/CeSiO₂ perovskite-type oxides for the production of hydrogen. *Appl. Catal. A Gen.* **2016**, *520*, 53–64. [[CrossRef](#)]
14. Calles, J.; Carrero, A.; Vizcaíno, A.; Lindo, M. Effect of Ce and Zr addition to Ni/SiO₂ catalysts for hydrogen production through ethanol steam reforming. *Catalysts* **2015**, *5*, 58–76. [[CrossRef](#)]
15. De Lima, S.M.; da Silva, A.M.; da Costa, L.O.O.; Graham, U.M.; Jacobs, G.; Davis, B.H.; Mattos, L.V.; Noronha, F.B. Study of catalyst deactivation and reaction mechanism of steam reforming, partial oxidation, and oxidative steam reforming of ethanol over Co/CeO₂ catalyst. *J. Catal.* **2009**, *268*, 268–281. [[CrossRef](#)]
16. Nabgan, W.; Tuan Abdullah, T.A.; Mat, R.; Nabgan, B.; Gambo, Y.; Tri wahyono, S. Influence of Ni to Co ratio supported on ZrO₂ catalysts in phenol steam reforming for hydrogen production. *Int. J. Hydrogen Energy* **2016**, *41*, 22922–22931. [[CrossRef](#)]

17. De Lima, A.E.P.; de Oliveira, D.C. In situ XANES study of cobalt in Co-Ce-Al catalyst applied to steam reforming of ethanol reaction. *Catal. Today* **2017**, *283*, 104–109. [[CrossRef](#)]
18. Cifuentes, B.; Hernández, M.; Monsalve, S.; Cobo, M. Hydrogen production by steam reforming of ethanol on a RhPt/CeO₂/SiO₂ catalyst: Synergistic effect of the Si:Ce ratio on the catalyst performance. *Appl. Catal. A Gen.* **2016**, *523*, 283–293. [[CrossRef](#)]
19. Wang, Z.; Wang, C.; Chen, S.; Liu, Y. Co–Ni bimetal catalyst supported on perovskite-type oxide for steam reforming of ethanol to produce hydrogen. *Int. J. Hydrogen Energy* **2014**, *39*, 5644–5652. [[CrossRef](#)]
20. Romero-Sarria, F.; Vargas, J.C.; Roger, A.-C.; Kiennemann, A. Hydrogen production by steam reforming of ethanol: Study of mixed oxide catalysts Ce₂Zr_{1.5}Me_{0.5}O₈: Comparison of Ni/Co and effect of Rh. *Catal. Today* **2008**, *133*, 149–153. [[CrossRef](#)]
21. Vizcaíno, A.J.; Carrero, A.; Calles, J.A. Hydrogen production by ethanol steam reforming over Cu–Ni supported catalysts. *Int. J. Hydrogen Energy* **2007**, *32*, 1450–1461. [[CrossRef](#)]
22. Wang, F.; Li, Y.; Cai, W.; Zhan, E.; Mu, X.; Shen, W. Ethanol steam reforming over Ni and Ni–Cu catalysts. *Catal. Today* **2009**, *146*, 31–36. [[CrossRef](#)]
23. Palma, V.; Ruocco, C.; Castaldo, F.; Ricca, A.; Boettge, D. Ethanol steam reforming over bimetallic coated ceramic foams: Effect of reactor configuration and catalytic support. *Int. J. Hydrogen Energy* **2015**, *40*, 12650–12662. [[CrossRef](#)]
24. Moraes, T.S.; Neto, R.C.R.; Ribeiro, M.C.; Mattos, L.V.; Kourtelesis, M.; Ladas, S.; Verykios, X.; Bellot Noronha, F. The study of the performance of PtNi/CeO₂-nanocube catalysts for low temperature steam reforming of ethanol. *Catal. Today* **2015**, *242*, 35–49. [[CrossRef](#)]
25. Chiou, J.Y.Z.; Lee, C.-L.; Ho, K.-F.; Huang, H.-H.; Yu, S.-W.; Wang, C.-B. Catalytic performance of Pt-promoted cobalt-based catalysts for the steam reforming of ethanol. *Int. J. Hydrogen Energy* **2014**, *39*, 5653–5662. [[CrossRef](#)]
26. Kugai, J.; Subramani, V.; Song, C.; Engelhard, M.H.; Chin, Y.-H. Effects of nanocrystalline CeO₂ supports on the properties and performance of Ni–Rh bimetallic catalyst for oxidative steam reforming of ethanol. *J. Catal.* **2006**, *238*, 430–440. [[CrossRef](#)]
27. Pereira, E.B.; Homs, N.; Martí, S.; Fierro, J.L.G.; Ramírez de la Piscina, P. Oxidative steam-reforming of ethanol over Co/SiO₂, Co-Rh/SiO₂ and Co–Ru/SiO₂ catalysts: Catalytic behavior and deactivation/regeneration processes. *J. Catal.* **2008**, *257*, 206–214. [[CrossRef](#)]
28. Mondal, T.; Pant, K.K.; Dalai, A.K. Catalytic oxidative steam reforming of bio-ethanol for hydrogen production over Rh promoted Ni/CeO₂–ZrO₂ catalyst. *Int. J. Hydrogen Energy* **2015**, *40*, 2529–2544. [[CrossRef](#)]
29. Osorio-Vargas, P.; Campos, C.H.; Navarro, R.M.; Fierro, J.L.G.; Reyes, P. Rh/Al₂O₃–La₂O₃ catalysts promoted with CeO₂ for ethanol steam reforming reaction. *J. Mol. Catal. A Chem.* **2015**, *407*, 169–181. [[CrossRef](#)]
30. Han, S.J.; Bang, Y.; Yoo, J.; Park, S.; Kang, K.H.; Choi, J.H.; Song, J.H.; Song, I.K. Hydrogen production by steam reforming of ethanol over P123-assisted mesoporous Ni-Al₂O₃–ZrO₂ xerogel catalysts. *Int. J. Hydrogen Energy* **2014**, *39*, 10445–10453. [[CrossRef](#)]
31. Konsolakis, M.; Ioakimidis, Z.; Kraia, T.; Marnellos, G. Hydrogen production by ethanol steam reforming (ESR) over CeO₂ supported transition metal (Fe, Co, Ni, Cu) catalysts: Insight into the structure-activity relationship. *Catalysts* **2016**, *6*, 39. [[CrossRef](#)]
32. Yu, S.-W.; Huang, H.-H.; Tang, C.-W.; Wang, C.-B. The effect of accessible oxygen over Co₃O₄–CeO₂ catalysts on the steam reforming of ethanol. *Int. J. Hydrogen Energy* **2014**, *39*, 20700–20711. [[CrossRef](#)]
33. Cifuentes, B.; Valero, M.; Conesa, J.; Cobo, M. Hydrogen production by steam reforming of ethanol on Rh–Pt catalysts: Influence of CeO₂, ZrO₂, and La₂O₃ as supports. *Catalysts* **2015**, *5*, 1872–1896. [[CrossRef](#)]
34. Srisiriwat, N.; Therdthianwong, S.; Therdthianwong, A. Oxidative steam reforming of ethanol over Ni/Al₂O₃ catalysts promoted by CeO₂, ZrO₂ and CeO₂–ZrO₂. *Int. J. Hydrogen Energy* **2009**, *34*, 2224–2234. [[CrossRef](#)]
35. Shanmugam, V.; Zapf, R.; Neuberg, S.; Hessel, V.; Kolb, G. Effect of ceria and zirconia promoters on Ni/SBA-15 catalysts for coking and sintering resistant steam reforming of propylene glycol in microreactors. *Appl. Catal. B Environ.* **2017**, *203*, 859–869. [[CrossRef](#)]
36. Palma, V.; Ruocco, C.; Meloni, E.; Gallucci, F.; Ricca, A. Enhancing Pt–Ni/CeO₂ performances for ethanol reforming by catalyst supporting on high surface silica. *Catal. Today* **2017**. [[CrossRef](#)]
37. Viviente, J.L.; Meléndez, J.; Pacheco Tanaka, D.A.; Gallucci, F.; Spallina, V.; Manzolini, G.; Foresti, S.; Palma, V.; Ruocco, C.; Roses, L. Advanced m-CHP fuel cell system based on a novel bio-ethanol fluidized bed membrane reformer. *Int. J. Hydrogen Energy* **2017**, *42*, 13970–13987. [[CrossRef](#)]

38. Ruocco, C.; Meloni, E.; Palma, V.; van Sint Annaland, M.; Spallina, V.; Gallucci, F. Pt-Ni based catalyst for ethanol reforming in a fluidized bed membrane reactor. *Int. J. Hydrogen Energy* **2016**, *41*, 20122–20136. [[CrossRef](#)]
39. Qin, H.; Qian, X.; Meng, T.; Lin, Y.; Ma, Z. Pt/MO_x/SiO₂, Pt/MO_x/TiO₂, and Pt/MO_x/Al₂O₃ Catalysts for CO oxidation. *Catalysts* **2015**, *5*, 606–633. [[CrossRef](#)]
40. Cecilia, J.; Arango-Díaz, A.; Marrero-Jerez, J.; Núñez, P.; Moretti, E.; Storaro, L.; Rodríguez-Castellón, E. Catalytic behaviour of CuO-CeO₂ systems prepared by different synthetic methodologies in the CO-PROX reaction under CO₂-H₂O feed stream. *Catalysts* **2017**, *7*, 160. [[CrossRef](#)]
41. Vizcaíno, A.J.; Lindo, M.; Carrero, A.; Calles, J.A. Hydrogen production by steam reforming of ethanol using Ni catalysts based on ternary mixed oxides prepared by coprecipitation. *Int. J. Hydrogen Energy* **2012**, *37*, 1985–1992. [[CrossRef](#)]
42. Dong, X.; Song, M.; Jin, B.; Zhou, Z.; Yang, X. The synergy effect of Ni-M (M = Mo, Fe, Co, Mn or Cr) bicomponent catalysts on partial methanation coupling with water gas shift under low H₂/CO conditions. *Catalysts* **2017**, *7*, 51–68. [[CrossRef](#)]
43. Chiou, J.Y.Z.; Siang, J.-Y.; Yang, S.-Y.; Ho, K.-F.; Lee, C.-L.; Yeh, C.-T.; Wang, C.-B. Pathways of ethanol steam reforming over ceria-supported catalysts. *Int. J. Hydrogen Energy* **2012**, *37*, 13667–13673. [[CrossRef](#)]
44. Palma, V.; Castaldo, F.; Ciambelli, P.; Iaquaniello, G.; Capitani, G. On the activity of bimetallic catalysts for ethanol steam reforming. *Int. J. Hydrogen Energy* **2013**, *38*, 6633–6645. [[CrossRef](#)]
45. Mondal, T.; Pant, K.K.; Dalai, A.K. Oxidative and non-oxidative steam reforming of crude bio-ethanol for hydrogen production over Rh promoted Ni/CeO₂-ZrO₂ catalyst. *Appl. Catal. A Gen.* **2015**, *499*, 19–31. [[CrossRef](#)]
46. Luisetto, I.; Tuti, S.; Di Bartolomeo, E. Co and Ni supported on CeO₂ as selective bimetallic catalyst for dry reforming of methane. *Int. J. Hydrogen Energy* **2012**, *37*, 15992–15999. [[CrossRef](#)]
47. Rico-Pérez, V.; Aneggi, E.; Trovarelli, A. The effect of Sr addition in Cu- and Fe-modified CeO₂ and ZrO₂ soot combustion catalysts. *Catalysts* **2017**, *7*, 28–40. [[CrossRef](#)]
48. Ay, H.; Üner, D. Dry reforming of methane over CeO₂ supported Ni, Co and Ni-Co catalysts. *Appl. Catal. B Environ.* **2015**, *179*, 128–138. [[CrossRef](#)]
49. Ocsachoque, M.A.; Eugenio Russman, J.I.; Irigoyen, B.; Gazzoli, D.; González, M.G. Experimental and theoretical study about sulfur deactivation of Ni/CeO₂ and Rh/CeO₂ catalysts. *Mater. Chem. Phys.* **2016**, *172*, 69–76. [[CrossRef](#)]
50. Italiano, C.; Balzarotti, R.; Vita, A.; Latorrata, S.; Fabiano, C.; Pino, L.; Cristiani, C. Preparation of structured catalysts with Ni and Ni-Rh/CeO₂ catalytic layers for syngas production by biogas reforming processes. *Catal. Today* **2016**, *273*, 3–11. [[CrossRef](#)]
51. Pérez-Hernández, R.; Gutiérrez-Martínez, A.; Palacios, J.; Vega-Hernández, M.; Rodríguez-Lugo, V. Hydrogen production by oxidative steam reforming of methanol over Ni/CeO₂-ZrO₂ catalysts. *Int. J. Hydrogen Energy* **2011**, *36*, 6601–6608. [[CrossRef](#)]
52. Pastor-Pérez, L.; Buitrago-Sierra, R.; Sepúlveda-Escribano, A. CeO₂-promoted Ni/activated carbon catalysts for the water-gas shift (WGS) reaction. *Int. J. Hydrogen Energy* **2014**, *39*, 17589–17599. [[CrossRef](#)]
53. Liu, Y.; Misono, M. Hydroisomerization of n-Butane over platinum-promoted cesium hydrogen salt of 12-tungstophosphoric acid. *Materials* **2009**, *2*, 2319–2336. [[CrossRef](#)]
54. Gould, T.D.; Montemore, M.M.; Lubers, A.M.; Ellis, L.D.; Weimer, A.W.; Falconer, J.L.; Medlin, J.W. Enhanced dry reforming of methane on Ni and Ni-Pt catalysts synthesized by atomic layer deposition. *Appl. Catal. A Gen.* **2015**, *492*, 107–116. [[CrossRef](#)]
55. Zhou, L.; Guo, Y.; Kameyama, H.; Bassett, J.-M. An anodic alumina supported Ni-Pt bimetallic plate-type catalysts for multi-reforming of methane, kerosene and ethanol. *Int. J. Hydrogen Energy* **2014**, *39*, 7291–7305. [[CrossRef](#)]
56. Mei, Z.; Li, Y.; Fan, M.; Zhao, L.; Zhao, J. Effect of the interactions between Pt species and ceria on Pt/ceria catalysts for water gas shift: The XPS studies. *Chem. Eng. J.* **2015**, *259*, 293–302. [[CrossRef](#)]
57. Turchetti, L.; Murmura, M.A.; Monteleone, G.; Giaconia, A.; Lemonidou, A.A.; Angeli, S.D.; Palma, V.; Ruocco, C.; Annesini, M.C. Kinetic assessment of Ni-based catalysts in low-temperature methane/biogas steam reforming. *Int. J. Hydrogen Energy* **2016**, *41*, 16865–16877. [[CrossRef](#)]
58. Kundakovic, L.; Flytzani-Stephanopoulos, M. Reduction characteristics of copper oxide in cerium and zirconium oxide systems. *Appl. Catal. A Gen.* **1998**, *171*, 13–29. [[CrossRef](#)]

59. Vicente, J.; Ereña, J.; Montero, C.; Azkoiti, M.J.; Bilbao, J.; Gayubo, A.G. Reaction pathway for ethanol steam reforming on a Ni/SiO₂ catalyst including coke formation. *Int. J. Hydrogen Energy* **2014**, *39*, 18820–18834. [CrossRef]
60. Moretti, E.; Storaro, L.; Talon, A.; Chitsazan, S.; Garbarino, G.; Busca, G.; Finocchio, E. Ceria-zirconia based catalysts for ethanol steam reforming. *Fuel* **2015**, *153*, 166–175. [CrossRef]
61. Zhao, L.; Han, T.; Wang, H.; Zhang, L.; Liu, Y. Ni-Co alloy catalyst from LaNi_{1-x}Co_xO₃ perovskite supported on zirconia for steam reforming of ethanol. *Appl. Catal. B Environ.* **2016**, *187*, 19–29. [CrossRef]
62. Sanchez-Sanchez, M.C.; Navarro Yerga, R.M.; Kondarides, D.I.; Verykios, X.E.; Fierro, J.L.G. Mechanistic aspects of the ethanol steam reforming reaction for hydrogen production on Pt, Ni, and PtNi catalysts supported on γ-Al₂O₃. *J. Phys. Chem. A* **2010**, *114*, 3873–3882. [CrossRef] [PubMed]
63. García-Díéguez, M.; Finocchio, E.; Larrubia, M.Á.; Alemany, L.J.; Busca, G. Characterization of alumina-supported Pt, Ni and PtNi alloy catalysts for the dry reforming of methane. *J. Catal.* **2010**, *274*, 11–20. [CrossRef]
64. Morales, M.; Segarra, M. Steam reforming and oxidative steam reforming of ethanol over La_{0.6}Sr_{0.4}CoO_{3-δ} perovskite as catalyst precursor for hydrogen production. *Appl. Catal. A Gen.* **2015**, *502*, 305–311. [CrossRef]
65. Peela, N.R.; Kunzru, D. Oxidative steam reforming of ethanol over Rh based catalysts in a micro-channel reactor. *Int. J. Hydrogen Energy* **2011**, *36*, 3384–3396. [CrossRef]
66. Vicente, J.; Montero, C.; Ereña, J.; Azkoiti, M.J.; Bilbao, J.; Gayubo, A.G. Coke deactivation of Ni and Co catalysts in ethanol steam reforming at mild temperatures in a fluidized bed reactor. *Int. J. Hydrogen Energy* **2011**, *39*, 12586–12596. [CrossRef]
67. Montero, C.; Ochoa, A.; Castaño, P.; Bilbao, J.; Gayubo, A.G. Monitoring Ni⁰ and coke evolution during the deactivation of a Ni/La₂O_{3-α}Al₂O₃ catalyst in ethanol steam reforming in a fluidized bed. *J. Catal.* **2015**, *331*, 181–192. [CrossRef]
68. Palma, V.; Ruocco, C.; Ricca, A. Bimetallic Pt and Ni based foam catalysts for low-temperature ethanol steam reforming intensification. *Chem. Eng. Trans.* **2015**, *43*, 559–564.
69. Muñoz, M.; Moreno, S.; Molina, R. Promoter effect of Ce and Pr on the catalytic stability of the Ni-Co system for the oxidative steam reforming of ethanol. *Appl. Catal. A Gen.* **2016**, *526*, 84–94. [CrossRef]
70. Palma, V.; Ruocco, C.; Ricca, A. Ceramic foams coated with Pt-Ni/CeO₂-ZrO₂ for bioethanol steam reforming. *Int. J. Hydrogen Energy* **2016**, *41*, 11526–11536. [CrossRef]



© 2017 by the authors. Licensee MDPI, Basel, Switzerland. This article is an open access article distributed under the terms and conditions of the Creative Commons Attribution (CC BY) license (<http://creativecommons.org/licenses/by/4.0/>).